# Lattice-Mismatch-Induced Twinning for Seeded Growth of Anisotropic Nanostructures

**Zhenni Wang,[†] Zhengzheng Chen,[†] Hui Zhang,[‡] Zhaorui Zhang,[†] Haijun Wu,[†] Mingshang Jin,[*,†] Chao Wu,[*,†] Deren Yang,[‡] and Yadong Yin[*,§]**

[†]Frontier Institute of Science and Technology and State Key Laboratory for Mechanical Behavior of Materials, Xi'an Jiaotong University, Xi'an, Shaanxi 710054, China, [‡]State Key Lab of Silicon Materials, Department of Materials Science and Engineering, Zhejiang University, Hangzhou, Zhejiang 310027, China, and [§]Department of Chemistry, University of California, Riverside, California 92521, United States

**ABSTRACT** Synthesis of anisotropic nanostructures from materials with isotropic crystal structures often requires the use of seeds containing twin planes to break the crystalline symmetry and promote the preferential anisotropic growth. Controlling twinning in seeds is therefore critically important for high-yield synthesis of many anisotropic nanostructures. Here, we demonstrate a unique strategy to induce twinning in metal nanostructures for anisotropic growth by taking advantage of the large lattice mismatch between two metals. By using Au—Cu as an example, we show, both theoretically and experimentally, that deposition of Cu to the surface of single-crystalline Au seeds can build up strain energy, which effectively induces the formation of twin planes. Subsequent seeded growth allows the production of Cu nanorods with high shape anisotropy that is unachievable without the use of Au seeds. This work provides an effective strategy for the preparation of anisotropic metal nanostructures.

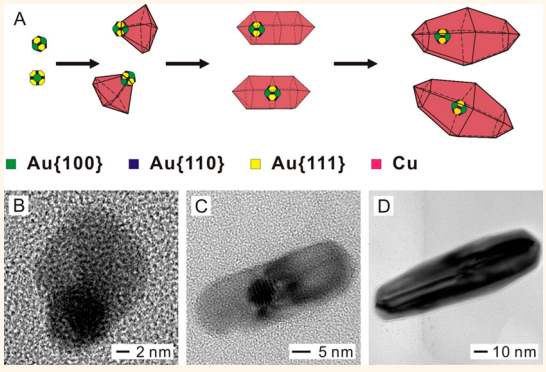


**KEYWORDS:** gold · copper · lattice mismatch · epitaxial growth · core—shell · twinned structure

Anisotropic metal nanostructures are a class of materials with unique shape-dependent properties and functionalities.[1−4] Their anisotropy in shape offers features and functions that are difficult to obtain simply by size-tuning, and thus promises their potential utilization in a number of important applications ranging from catalysis to imaging and sensing.[5−7] However, as most metals have a highly symmetric face-centered-cubic (fcc) crystal structure, forcing metal colloidal particles to acquire an anisotropic shape remains a great challenge. Recent studies indicate that twinning plays a critical role in forming anisotropic nanostructures.[8−10] According to Lofton and Sigmund, the formation of twin planes in the seed particles helps to break the crystalline symmetry and promote the anisotropic growth of metal nanoparticles.[8] Therefore, it has been widely agreed that a reliable strategy toward the synthesis of anisotropic metal nanostructures is to control the formation of seeds with the desired twin planes during the nucleation stage. However, a practical difficulty is that a typical synthesis often produces a mixture of single-crystalline, singly twin, and multiply twin seeds. It has been possible to obtain single-crystalline seeds with high purity by selectively removing the twin seeds by taking advantage of the relatively lower stability of the twin seeds against etchants such as the combination of halogen ions and $O_2$.[11] Many single-crystalline metal nanostructures with well-defined shapes (*e.g.*, octahedrons, cuboctahedrons, and cubes) can be subsequently produced from such seeds by simply controlling the growth kinetics. On the other hand, obtaining twin seeds in high quality still remains a major challenge, making it difficult to produce anisotropic nanostructures at high yield, especially those containing twins, by following similar processes for growing single-crystalline particles. Here we report that lattice mismatch between two metals can be utilized to effectively induce the

* Address correspondence to mingshangjin@gmail.com, chaowu@mail.xjtu.edu.cn, yadong.yin@ucr.edu.

Received for review January 22, 2015 and accepted March 5, 2015.

**Published online March 06, 2015**
10.1021/acsnano.5b00475

formation of twin planes in seeds, thus enabling their further growth into anisotropically shaped metal nanostructures at a significantly high yield.

We demonstrate the proposed strategy by using Cu and Au as the model system because these two metals are known to have a large lattice mismatch ($\delta$ = 11.4%). Scanning tunneling microscope (STM) studies have already revealed that the deposition of Cu can give rise to the formation of twin planes on a single-crystalline Au(100) substrate.[12] It is therefore expected that twinning may also occur during the deposition of Cu to colloidal single-crystalline Au seeds. In the formation of heterogeneous core−shell nanoparticles, the layered epitaxial growth mode is conventionally considered to be hindered when $\delta$ is larger than 5%.[13] Recently, however, we have successfully generated Pd@Cu core−shell nanocubes with $\delta$ = 7.1% *via* localized epitaxial growth mode, slightly violating the aforementioned criterion.[14] Different from the conventional growth behavior, the localized epitaxial growth mode allows Cu islands to initially nucleate at different sites on Pd seeds and then further grow until the entire surface of seeds is fully covered by Cu shells. When $\delta$ is even larger, as in the case of Au@Cu core−shell nanoparticles, crystalline defects such as twinning are expected to form eventually, thus offering new opportunities for constructing twin nanostructures on single-crystalline seeds and further promoting anisotropic growth.

## RESULTS AND DISCUSSION

To explore the effects of $\delta$ between shell and seed metals during seeded growth, we systematically studied the deposition of Cu on Au seeds by first-principles (FP) simulations. Previous theoretical studies have well explained twinning in binary alloys due to the nucleation of Shockley partial dislocations on several adjacent {111} planes. However, unlike this study, crystals are required before the twin formation.[15−19] In addition, considering the small sizes of Cu−Au when twinning is first observed, it is hard to believe that multiple partial dislocations can nucleate. Therefore, from a new theoretical perspective, we propose the conjugated orientation model.

A single-crystalline Au seed is typically enclosed by three facets, *i.e.*, {111}, {100}, and {110}, with {110} being the most energetic facet. Consistently, it has been found that {220} facets are also the most active sites during the initial deposition of Cu on the Au surface.[20] We therefore build the growth model by stacking Cu atoms on an Au {220} plane. There are two possible growing orientations of the deposited Cu multilayers (MLs). One is $[1\bar{1}0]_{Au}//[1\bar{1}0]_{Cu}$, referred to as collinear orientation (CL, shown in Figure 1A and Figure S1). In this orientation, Cu MLs simply follow the stacking sequence of the Au substrate and lead to conformal single-crystal coatings only. The other is

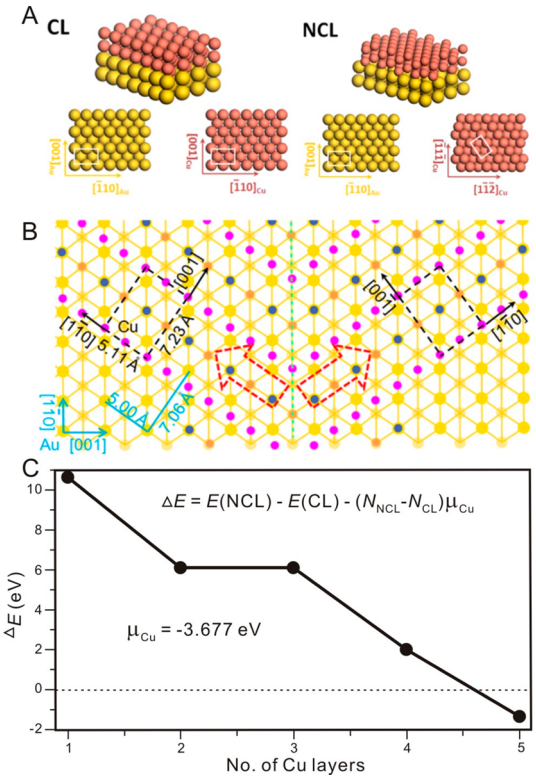


**Figure 1. (A) Collinear (CL) and noncollinear (NCL) growth model of Cu atoms on Au. Cu atoms are in orange, and Au atoms are in yellow. (B) Scheme of Cu twin on Au(110). Twin crystals are indicated by the two dashed red arrows. Au atoms in the top layer and sublayer are big and small yellow circles, respectively. Cu atoms are presented at atop sites (dark blue dots), 4-fold sites (orange dots), and bridge sites (magenta dots). Black broken lines define (2 × 1) Cu cells. Periods of Cu and Au along key directions are given as well. (C) Relative stable energy of CL *versus* NCL growth of Cu.**

noncollinear orientation (NCL, shown in Figure 1A and Figure S2), in which two conjugate alignments are possible: $[1\bar{1}0]_{Au}//[1\bar{1}2]_{Cu}$ and $[1\bar{1}0]_{Au}//[1\bar{1}\bar{2}]_{Cu}$, as shown by the two dashed red arrows in Figure 1B. When the two parts with different NCL alignments meet on the substrate, a twin boundary forms along $[1\bar{1}0]_{Au}$, as indicated by the green line. We treat the Au@Cu system as grand canonical ensembles; thus CL and NCL orientations are allowed to contain different numbers of Cu atoms. Note that in our supercell there are 24 and 18 Cu atoms per layer in NCL and CL orientations, respectively. In order to compare the relative stability of these two orientations, we define the relative stable energy $\Delta E$ as

$$\Delta E = E(\mathrm{NCL}) - E(\mathrm{CL}) - (N_{\mathrm{NCL}} - N_{\mathrm{CL}})\mu_{\mathrm{Cu}}$$

where $N_{NCL}$ and $N_{CL}$ are the numbers of Cu atoms in two orientations, and $\mu_{Cu}$ = −3.677 eV is the chemical potential of Cu since the Au@Cu system is assumed to be in equilibrium with bulk Cu. In this case, negative $\Delta E$ indicates a more stable NCL orientation.

Figure 1C presents $\Delta E$ as a function of Cu shell thickness (for side view of each configuration see Figure S3). $\Delta E$ decreases as the Cu MLs deposit onto

the Au substrate. For the first two MLs, the CL orientation is more stable. After depositing five Cu MLs, $\Delta E$ becomes negative, indicating that the NCL orientation becomes energetically more favorable. Therefore, the deposition of the initial four layers of Cu shell follows the CL orientation and subsequently switches to NCL once more than five layers of Cu atoms are grown on the surface of Au seeds. Due to the energetic degeneracy, deposited Cu MLs along the two conjugate NCL directions can coexist in the form of islands on the Au substrate. A twin boundary can therefore form if the two islands expand and eventually meet each other.

We need to further understand the behavior of $\Delta E$. Structural analysis shows that there are three kinds of adsorption sites over the Au(110) substrate: 4-fold, atop, and bridge (Figure S3). FP results demonstrate that Cu atoms at atop and bridge sites are less stable compared with those at 4-fold sites. In the CL orientation, all Cu atoms locate at 4-fold sites, while in the NCL orientation, 25% of Cu atoms are at atop sites, 50% are at bridge sites, and only 25% locate at 4-fold sites. On the other hand, $\delta$ between Au and Cu (11.4%) will induce strain energy in Cu MLs. The Cu MLs depositing in CL orientation will experience 11.4% biaxial strain and thus accumulate higher strain energy with the increase of the Cu thickness. As shown in Figure 1, Cu MLs in NCL orientation fit much better on the Au substrate: the biaxial mismatch is only ~2.1%. Consequently, there are two competing factors determining the stability of Cu MLs in different orientations: (1) the strain energy induced by $\delta$ and (2) the binding energy of Cu atoms at different sites. When the Cu shell is thin, CL orientation is more stable because of the stronger adsorption of Cu atoms at 4-fold sites than atop or bridge sites. With increasing Cu shell thickness, the CL orientation is less favorable due to the strain energy accumulation. When the strain energy is high enough to compensate the adsorption energy, the stable configuration of the Cu shell transits to the NCL orientation. The critical thickness is five Cu MLs according to our calculations. Note that if we take a different reference state of Cu ($\mu_{Cu}$ is different from −3.677 eV), the critical number of shells might be different, but the above discussions are still valid. In their study on the deposition behavior of Cu on a Au(100) substrate using STM technique, Kolb *et al.* have shown that only exactly 10 layers of Cu can be grown on a Au(100) substrate along the CL orientation. With the 11th layer, a structural transition suddenly takes place, which causes buckling of the Cu surface. In their study, the emerging new surface structures exhibit small domains rotated by 90° from each other due to the symmetry of Au(100), resulting in singly twin structure of Cu.[12] It is reasonable to expect that the deposition of Cu on colloidal Au seeds would prefer NCL orientation deposition, making it possible to form twin structures that are desired for anisotropic growth.

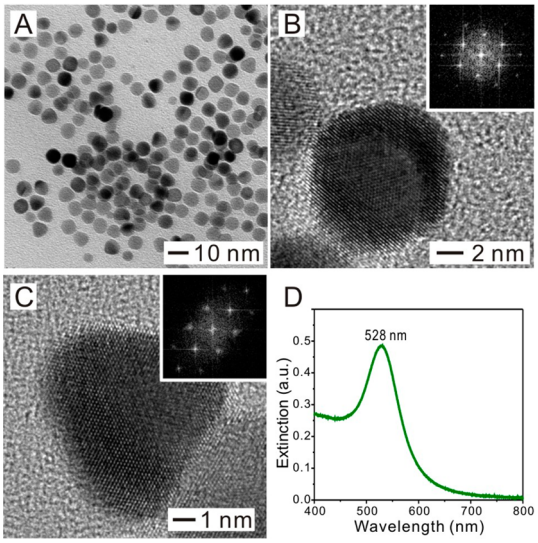


**Figure 2. (A) TEM image, (B, C) HRTEM images, and (D) UV−vis spectrum of Au nanoparticles serving as seeds. The insets in (B) and (C) show the corresponding Fourier transform pattern.**

When $\delta$ is relatively small, as in the case of Pd shells on Cu seeds, the system may still follow the conventional epitaxial growth mode. The $\delta$ between Cu MLs and the Pd substrate in CL and NCL orientations is 7.1% and 6.9%, respectively. Since the mismatches in two orientations are similar, adsorption energy becomes dominant. Cu MLs are always more stable in CL orientation and will not nucleate into twin structure. As evidence, the structural relaxation using the FP methods failed if the Cu shell is thicker than 2 MLs in NCL orientation on the Pd(110) substrate, suggesting that NCL orientation is not favored on Pd seeds. Thus, the overgrowth of Cu shells on Pd nanocubes at the same condition will result in the formation of Pd@Cu core−shell nanocubes, with Cu shells being epitaxially deposited onto Pd seeds along the same orientation, which is consistent with our reported work on Pd@Cu nanocubes.[14] Based on FP calculations and above discussions, we confirm that it is the appropriate $\delta$ between shell and seed metals that causes the twinning. More importantly, our results suggest a practically effective method for creating and controlling twin structures.

The simulation results indicate that it might be possible to achieve Cu twin planes on Au single-crystalline substrates/seeds resulting from their large $\delta$. To verify these theoretical predictions, single-crystalline Au nanospheres were first synthesized by following a previously reported two-step method and then used for seeded growth of Cu shells.[21] According to the literature; the spheres prepared through this method were in fact cuboctahedrons. Figure 2 shows the transmission electron microscopy (TEM) images of the as-prepared Au nanocrystals, as well as their corresponding ultraviolet−visible (UV−vis) spectrum. From

TEM image in Figure 2A, it is clear that pseudospherical Au nanoparticles (cuboctahedrons) are the dominant (>80%) products, with a small fraction in the tetrahedral shape. The final nanoparticles contained ~94% of single-crystalline seeds, together with ~6% of twinned seeds (Figure S4). All nanoparticles have a uniform size of *ca*. 11 nm. High-resolution TEM (HRTEM) and Fourier transform (FT) patterns confirm that these Au nanoparticles are single-crystalline regardless of shapes, as shown in Figure 2B and C. A localized surface plasmon resonance (LSPR) peak is located at 528 nm (Figure 2D), consistent with previous reports on Au nanoparticles with similar sizes.[22,23]

These single-crystalline Au nanoparticles were then used as the seeds to induce the localized epitaxial growth of Cu shells upon the reduction of $CuCl_2$ by glucose in the presence of hexadecylamine (HDA).[14,24] As shown in the representative scanning electron microscopy (SEM) and TEM images in Figure 3, the products resulting from the seeded growth are Au@Cu nanorods with high shape uniformity and high yield. Apparently, the large $\delta$ (11.4%) has a significant impact on the epitaxial growth of heterostructures in solution,[25] and it is responsible for the evolution from the pseudospherical seeds to the rod-shaped products. This result is remarkably consistent with our theoretical predictions. Careful observation of the SEM image further reveals some small holes with sizes around 30 nm on some nanorods. As an air-sensitive metal, Cu would be easily oxidized when exposed to the air without sufficient protection from surfactants. As a result, high-energy sites of the as-prepared Au@Cu core–shell nanorods, especially the interfaces of Au seeds and Cu shells, could be quickly oxidized after the surfactant is partially removed during washing, producing holes on the nanorods (marked by arrows in Figure 3A). We further applied energy-dispersive X-ray (EDX) line-scan analysis to determine the distribution of Au and Cu in the nanorods, as shown in Figure 3C. The Au signal was found at the core area with a size in good agreement with that of the original Au seeds. More direct evidence was obtained by EDX elemental mapping (Figure 3D), which clearly shows a distinct spherical Au core in a Cu nanorod, supporting the conclusion that Cu has been successfully deposited on Au seeds despite the large $\delta$ between these metals.

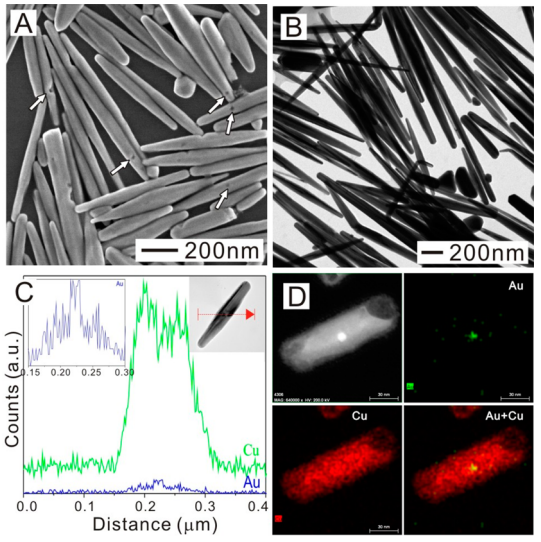


**Figure 3. (A) SEM, (B) TEM, and (C, D) EDX line-scan and mapping of Au@Cu nanorods prepared under standard conditions.**

In order to reveal the important role of twin planes in the anisotropic growth, the Au@Cu nanorods were further analyzed by bright- and dark-field TEM imaging as well as selected area electron diffraction (SAED). Figure 4 shows the results for Au@Cu core–shell nanorods with two typical orientations. Clearly, Au seeds can be identified inside the Cu nanorods (Figure 4A and E). The dark-field images in Figure 4B and F were taken from spots (220) selected by the objective lens aperture: light contrast along the long axis direction can be observed all over the nanorod in Figure 4B, while only

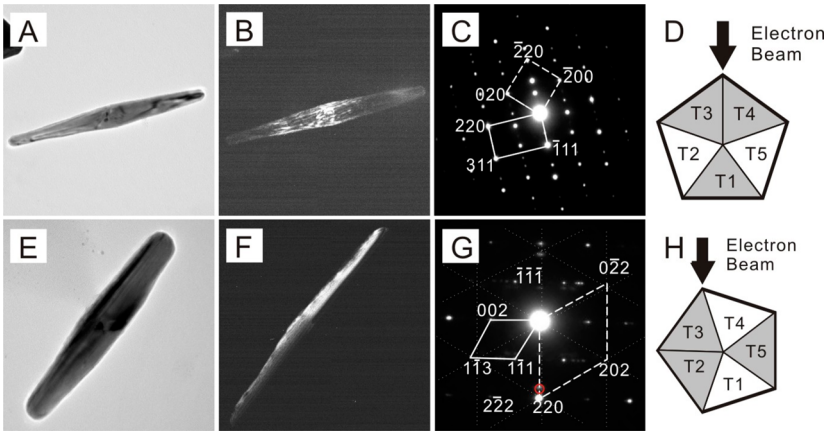


**Figure 4. Characterizations of two individual Au@Cu nanorods. (A, E) TEM, (B, F) dark-field images, and (C, G) SAED patterns. (D, H) Cross-sectional models of the Au@Cu nanorods showing arrangements of twins T1 to T5. The red circle in (G) shows the diffraction corresponds to the (220) facet of the Au seeds.**

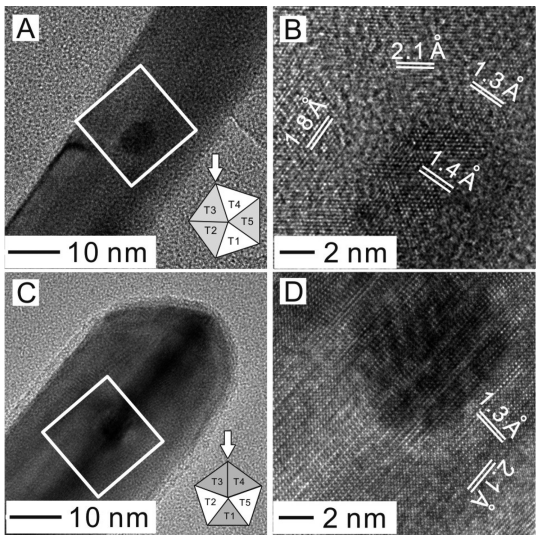


**Figure 5. (A, C) TEM and (B, D) HRTEM images of two individual nanorods along different orientations.**

half of the nanorod exhibits light contrast in Figure 4F due to the different orientations. These results indicate that the nanorods contain twins, which were further characterized by SAED analyses. As shown in Figure 4C and G, both diffraction patterns with different orientations indicate that Cu nanorods are crystallized in the fcc structure, but neither of them could be assigned to a single-crystalline structure. Most of the diffraction spots in Figure 4C can be indexed as the diffractions of the [$\bar{1}$12] and [001] zone axis (Figure 4D), while those in Figure 4G can be assigned to the [1$\bar{1}$0] and [1$\bar{1}\bar{1}$] zone axis (Figure 4H), suggesting that the Cu nanorods should possess a multiply twin structure. In fact, these observations are consistent with the previous results obtained for pentatwin nanorods of Au, Cu, Ag, and Pd.[26−29] We can therefore confirm a pentatwin fcc structure model with five {111} twin boundaries for the Cu nanorods grown on the single-crystalline seeds, with their longitudinal direction along ⟨110⟩.

Although our simulation was not able to clearly indicate the stepwise evolution to pentatwin structures, we were able to verify the pentatwin structure of the nanorods experimentally by HRTEM studies. Figure 5 shows the TEM and HRTEM images taken from the core portion of two different Au@Cu nanorods, respectively. The insets schematically illustrate the orientations of the nanorods relative to the incident electron beam (Figure 5A and C). The Au seeds are clearly identified at the core area of the nanorods. When the axis of the e-beam was parallel to one of the side faces of the pentagonal nanorod (Figure 5B), three sets of fringes with lattice spacings of 2.1, 1.8, and 1.3 Å were observed, corresponding to the {111}, {200}, and {220} planes of Cu, respectively. Figure 5D shows the HRTEM image taken from an Au@Cu nanorod oriented with the bottom side face perpendicular to the e-beam. The fringes with lattice spacings of 2.1 and 1.3 Å could also be

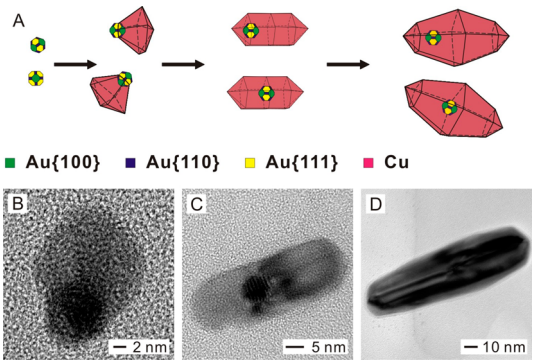


**Figure 6. (A) Proposed growth model and (B−D) TEM images of Cu shells on an Au single-crystalline seed obtained at 14, 22, and 36 h, respectively.**

assigned to the {111} and {220} planes of Cu, respectively. This result indicates that the Au@Cu nanorods were grown along the ⟨110⟩ direction. As well, the data further demonstrated the successful synthesis of the pentatwin structure of Cu shells on single-crystalline cores. Considering the pentatwin structured shells and the relatively thinner Cu layer at the core area (Figure S5), it is possible to observe the atomic arrangement of the initial deposited Cu layer on the Au seeds through HRTEM characterization. Since the Au core is positioned at the center of the nanorod, half of the Au core area in Figure 5B was covered by Cu lattice fringes. Interestingly, the distances of lattice fringes at the core area are slightly deviated from the theoretical Cu lattice constants. As marked in Figure 5B, the constants were measured to be 0.14 nm at the core area, which are larger than that of theoretical values (0.128 nm) of fcc Cu along the same direction. This enlargement is probably due to the influence of the Au core. Although Cu atoms are successfully deposited on Au cores with the same ⟨220⟩ direction, the growth still needs to bear additional stress to fit the lattice of Au, subsequently resulting in an increase in the lattice parameter of Cu. The same orientation of Au and Cu along ⟨220⟩ can be verified through SAED and moiré patterns. In addition to the associated double-diffraction reflections of pentatwin Cu shells in the SAED pattern, a second smaller set of diffraction spots from the Au core (Figure 4G, indicated by red cycles) can be assigned to the Au(220) epitaxially oriented with the ⟨110⟩ growth direction of Cu shells. Analysis of the moiré patterns [fringes covered the core area of some nanorods due to the superposition of two misfit crystalline lattices (Au and Cu lattices)] also confirms this orientation relationship (Figure S6). The lattice spacing shown in Figure S5 is 1.124 nm, corresponding to the calculated data (1.152 nm) of the crystal lattices of Au and Cu {220} planes. These results confirm that the Cu pentatwin shells have successfully grown onto Au single-crystalline seeds in an epitaxial manner by sharing common {220} planes.

To further understand the growth process of the pentatwin Cu shells, we took TEM images from a set of products at different reaction time so as to better

complement the simulation results (Figure 6). Initially, Cu atoms nucleate on one side of an Au particle and then grow into a large blob through localized epitaxial growth. The deposited Cu blob prefers to form a pentatwin structure to minimize the strain energy due to the large $\delta$ between Au and Cu (Figures 6B and S7). HRTEM imaging, however, could not clearly identify the pentatwin structure for Au−Cu bimetallic particles at the early stage. As the reaction proceeds, the pentatwin Cu blob slowly evolves into rod-shaped shells, as shown in Figure 6C. Eventually, the entire Au seed is encased, leading to Au@Cu core−shell nanorods (Figure 6D). The critical role of large lattice mismatch in the formation of twin nanostructures on single-crystalline seeds is also confirmed by two control experiments. First, without Au seeds, Cu nanocubes were obtained, consistent with the fcc crystalline nature of the metal (Figure S8). Second, when Pd nanocubes were introduced as seeds, Pd@Cu nanocubes were generated due to the relatively small lattice mismatch compared with the Au−Cu system (Figure S9), which is in agreement with our previous results.[14]

## CONCLUSION

In summary, we demonstrate a unique strategy to induce twinning in metal nanostructures for anisotropic growth by taking advantage of the large $\delta$ between two metals. By using Au−Cu as a model system, we show both theoretically and experimentally that the strain energy due to large $\delta$ can effectively induce the formation of twin planes on single-crystalline seeds and subsequently promote the anisotropic growth into nanorods. We believe this work provides a novel and highly effective strategy for the rational design and synthesis of anisotropic nanostructures from materials with intrinsic isotropic crystal structures.

## METHODS

**Experimental Section.** *Chemicals and Materials.* Gold chloride trihydrate ($HAuCl_4 \cdot 3H_2O$), sodium borohydride ($NaBH_4$), cetyltrimethylammonium bromide (CTAB), L-ascorbic acid (AA), copper chloride dehydrate ($CuCl_2 \cdot 2H_2O$), hexadecylamine (HDA), and glucose ($C_6H_{12}O_6$) were all obtained from Sigma-Aldrich.

*Synthesis of Au Seeds.* The Au nanoparticle seeds were prepared using a two-step procedure. We first synthesized 3 nm Au nanoparticles by adding 0.6 mL of ice-cold $NaBH_4$ solution (10 mM) into a 10 mL aqueous solution containing $HAuCl_4$ (0.25 mM) and CTAB (0.1 M), generating a brownish solution. The seed solution was kept undisturbed for 3 h at 27 °C to ensure complete decomposition of $NaBH_4$ remaining in the solution. After that, 6 mL of $HAuCl_4$ (0.5 mM), 6 mL of CTAB (0.2 M), and 4.5 mL of AA (0.1 M) aqueous solution were mixed, followed by the addition of 0.3 mL of the as-prepared 3 nm Au nanoparticles. The final mixture turned from colorless to red within 1 min, indicating the formation of large Au nanoparticles. After 1 h, a UV−vis spectrum was recorded from the Au nanoparticle suspension.

*Synthesis of Au@Cu Nanorods.* The Au−Cu nanorods were prepared using a seed-mediated method. In a typical synthesis, 21 mg of $CuCl_2 \cdot 2H_2O$ and 90 mg of HDA were mixed with 10 mL of water in a glass vial. This mixed solution was magnetically stirred at room temperature, and then 50 mg of glucose was added into the solution and stirred for 4 h, followed by the addition of 1 mL of the single-crystalline Au seeds. The vial was then transferred into an oil bath and heated at 80 °C for 36 h under magnetic stirring.

**Computational Methods.** The VASP code[30,31] with generalized gradient approximation for the exchange−correlation functionals (Perdew−Burke−Ernzerhof)[32] was used for all calculations. The geometric relaxation threshold was set to 0.02 eV/Å, and the electronic structure convergence was $10^{-4}$ eV. The energy cutoff of plane waves was 274 eV. The Methfessel−Paxton smearing method with a width of 0.05 eV was used. A $3 \times 3 \times 1$ Monkhorst−Pack k-point mesh was chosen.[33] As shown in Figure S1, a $3 \times 3$ Au(110) supercell with three layers was adopted as substrate. The bottom two layers were fixed throughout all calculations to mimic the bulk environment. Note that the $3 \times 3$ supercell is the smallest one that is compatible with periodicity of both CL and NCL orientations of the Cu shell. Cu atoms were added onto the Au substrate layer by layer. The thickness of the calculating box was 20.2 Å, so that even with the thickest Cu multilayers considered in the present work the vacuum was still 11.1 Å to separate the periodic slabs. The lattice constants of Au, Pd, and Cu were set to be the experimental value: 4.078, 3.891, and 3.615 Å, respectively.

**Characterizations.** Transmission electron microscopy, high-resolution TEM, selected-area electron diffraction, and dark-field and energy-dispersive X-ray analyses were performed using a JEOL 2100F microscope operated at 200 kV (Tokyo, Japan). UV−vis spectra were recorded with an Ocean Optics HR2000+ES UV−vis−NIR spectrophotometer with a DH-2000-BAL light source.

*Conflict of Interest:* The authors declare no competing financial interest.

*Supporting Information Available:* Model of a thin Cu layer at the Au core and collinear and noncollinear growth model of Cu atoms on Au and their relatively stable energy. The histogram of the percentage of single-crystalline nanoparticles. High-resolution TEM image of the moiré patterns in the Au−Cu nanorods and of Au@Cu nanorods at the initial stage. TEM images of nanocrystals obtained by using Pd nanocubes as seeds and without seeds at the same condition. This material is available free of charge *via* the Internet at http://pubs.acs.org.

*Acknowledgment.* Y.Y. thanks the U.S. National Science Foundation (CHE-1308587) for partial support of this research. M.J. is grateful for the financial support from National Natural Science Foundation of China (NSFC, Nos. 21403160 and 21471123) and the "start-up fund", "the Fundamental Research Funds for the Central Universities" provided by Xi'an Jiaotong University. C.W. acknowledges support from NSFC (21203143 and 21477096). H.Z. acknowledges financial support from the 973 Project (2013CB632100), NSFC (No. 5137222), and the Fundamental Research Funds for the Central Universities (No. 2014FZA4007). We also thank Materials Physics Center of FIST for providing computational resources.

## REFERENCES AND NOTES

1. Caswell, K. K.; Bender, C. M.; Murphy, C. J. Seedless, Surfactantless Wet Chemical Synthesis of Silver Nanowires. *Nano Lett.* **2003**, *3*, 667–669.
2. Kim, F.; Sohn, K.; Wu, J.; Huang, J. Chemical Synthesis of Gold Nanowires in Acidic Solutions. *J. Am. Chem. Soc.* **2008**, *130*, 14442–14443.
3. Henzie, J.; Kwak, E.-S.; Odom, T. W. Mesoscale Metallic Pyramids with Nanoscale Tips. *Nano Lett.* **2005**, *5*, 1199–1202.

4. Lee, J.; Hasan, W.; Stender, C. L.; Odom, T. W. Pyramids: A Platform for Designing Multifunctional Plasmonic Particles. *Acc. Chem. Res.* **2008**, *41*, 1762–1771.
5. Liao, H.; Hafner, J. H. Gold Nanorod Bioconjugates. *Chem. Mater.* **2005**, *17*, 4636–4641.
6. Rex, M.; Hernandez, F. E.; Campiglia, A. D. Pushing the Limits of Mercury Sensors with Gold Nanorods. *Anal. Chem.* **2005**, *78*, 445–451.
7. Takahashi, H.; Niidome, Y.; Yamada, S. Controlled Release of Plasmid DNA from Gold Nanorods Induced by Pulsed Near-Infrared Light. *Chem. Commun.* **2005**, 2247–2249.
8. Lofton, C.; Sigmund, W. Mechanisms Controlling Crystal Habits of Gold and Silver Colloids. *Adv. Funct. Mater.* **2005**, *15*, 1197–1208.
9. Bögels, G.; Meekes, H.; Bennema, P. Growth Mechanism of Vapor-Grown Silver Crystals: Relation between Twin Formation and Morphology. *J. Phys. Chem. B* **1999**, *103*, 7577–7583.
10. Elechiguerra, J. L.; Reyes-Gasqa, J.; Yacaman, M. J. The Role of Twinning in Shape Evolution of Anisotropic Noble Metal Nanostructures. *J. Mater. Chem.* **2006**, *16*, 3906–3919.
11. Wiley, B.; Herricks, T.; Sun, Y.; Xia, Y. Polyol Synthesis of Silver Nanoparticles: Use of Chloride and Oxygen to Promote the Formation of Single-Crystal, Truncated Cubes and Tetrahedrons. *Nano Lett.* **2004**, *4*, 1733–1739.
12. Randler, R. J.; Dietterle, M.; Kolb, D. M. The Initial Stages of Cu Deposition on Au(100) as Studied by *in-Situ* STM: The Epitaxial Growth of *bcc* Cu. *Z. Phys. Chem.* **1999**, *208*, 43–56.
13. Fan, F.; Liu, D.; Wu, Y.; Duan, S.; Xie, Z.; Jiang, Z.; Tian, Z. Epitaxial Growth of Heterogeneous Metal Nanocrystals: From Gold Nano-Octahedra to Palladium and Silver Nanocubes. *J. Am. Chem. Soc.* **2008**, *130*, 6949–6951.
14. Jin, M.; Zhang, H.; Wang, J.; Zhong, X.; Lu, N.; Li, Z.; Xie, Z.; Kim, M. J.; Xia, Y. Copper Can Still Be Epitaxially Deposited on Palladium Nanocrystals to Generate Core-Shell Nanocubes Despite Their Large Lattice Mismatch. *ACS Nano* **2012**, *6*, 2566–2573.
15. Van Swygenhoven, H.; Derlet, P. M.; Frøseth, A. G. Stacking Fault Energies and Slip in Nanocrystalline Metals. *Nat. Mater.* **2004**, *3*, 399–403.
16. Finkenstadt, D.; Johnson, D. D. Solute/Defect-Mediated Pathway for Rapid Nanoprecipitation in Solid Solutions: $\gamma$ Surface Analysis in *fcc* Al-Ag. *Phys. Rev. B* **2006**, *73*, 024101.
17. Kibey, S.; Liu, J. B.; Johnson, D. D.; Sehitoglu, H. Generalized Planar Fault Energies and Twinning in Cu−Al Alloys. *Appl. Phys. Lett.* **2006**, *89*, 191911.
18. Kibey, S.; Wang, L. L.; Liu, J. B.; Johnson, H. T.; Sehitoglu, H.; Johnson, D. D. Quantitative Prediction of Twinning Stress in *fcc* Alloys: Application to Cu-Al. *Phys. Rev. B* **2009**, *79*, 214202.
19. Kibey, S.; Liu, J. B.; Curtis, M. J.; Johnson, D. D.; Sehitoglu, H. Effect of Nitrogen on Generalized Stacking Fault Energy and Stacking Fault Widths in High Nitrogen Steels. *Acta Mater.* **2006**, *54*, 2991–3001.
20. Xia, Y.; Xiong, Y.; Lim, B.; Skrabalak, S. E. Shape-Controlled Synthesis of Metal Nanocrystals: Simple Chemistry Meets Complex Physics?. *Angew. Chem., Int. Ed.* **2008**, *48*, 60–103.
21. Ma, Y.; Li, W.; Cho, E. C.; Li, Z.; Yu, T.; Zeng, J.; Xie, Z.; Xia, Y. Au@Ag Core-Shell Nanocubes with Finely Tuned and Well-Controlled Sizes, Shell Thicknesses, and Optical Properties. *ACS Nano* **2010**, *4*, 6725–6734.
22. Polavarapu, L.; Xu, Q. A Simple Method for Large Scale Synthesis of Highly Monodisperse Gold Nanoparticles at Room Temperature and Their Electron Relaxation Properties. *Nanotechnology* **2009**, *20*, 185606.
23. Haiss, W.; Thanh, N. T. K.; Aveyard, J.; Fernig, D. G. Determination of Size and Concentration of Gold Nanoparticles from UV-Vis Spectra. *Anal. Chem.* **2007**, *79*, 4215–4221.
24. Jin, M.; He, G.; Zhang, H.; Zeng, J.; Xie, Z.; Xia, Y. Shape-Controlled Synthesis of Copper Nanocrystals in an Aqueous Solution with Glucose as a Reducing Agent and Hexadecylamine as a Capping Agent. *Angew. Chem., Int. Ed.* **2011**, *50*, 10560–10564.
25. Habas, S. E.; Lee, H.; Radmilovic, V.; Somorjai, G. A.; Yang, P. Shaping Binary Metal Nanocrystal through Epitaxial Seeded Growth. *Nat. Mater.* **2007**, *6*, 692–697.
26. Perez-Juste, J.; Pastoriza-Santos, I.; Liz-Marzan, L. M.; Mulvaney, P. Gold Nanorods: Synthesis, Characterization and Applications. *Coord. Chem. Rev.* **2005**, *249*, 1870–1901.
27. Zhang, S.; Jiang, Z.; Xie, Z.; Huang, R.; Zheng, L. Growth of Silver Nanowires from Solutions: A Cyclic Penta-Twinned-Crystal Growth Mechanism. *J. Phys. Chem. B* **2005**, *109*, 9416–9421.
28. Jin, M.; Kuang, Q.; Jiang, Z.; Xu, T.; Xie, Z.; Zheng, L. Direct Synthesis of Silver/Polymer/Carbon Nanocables *via* a Simple Hydrothermal Route. *J. Solid. State Chem.* **2008**, *181*, 2359–2363.
29. Huang, X. Q.; Zheng, N. F. One-Pot, High-Yield Synthesis of 5-Fold Twinned Pd Nanowires and Nanorods. *J. Am. Chem. Soc.* **2009**, *131*, 4602–4603.
30. Kresse, G.; Furthmüller, J. Efficient Iterative Schemes for *ab Initio* Total-Energy Calculations Using a Plane-Wave Basis Set. *Phys. Rev. B* **1996**, *54*, 11169–11186.
31. Kresse, G.; Furthmüller, J. *Vasp the Guide*; Institutfür Material-Physik, Universität Wien: Vienna, Austria, 2003.
32. Perdew, J. P.; Burke, K.; Ernzerhof, M. Generalized Gradient Approximation Made Simple. *Phys. Rev. Lett.* **1996**, *77*, 3865–3868.
33. Monkhorst, H. J.; Pack, J. D. Special Points for Brillouin-Zone Integrations. *Phys. Rev. B* **1976**, *13*, 5188–5192.